Design of a Novel Magnet Exhibiting Photoinduced Magnetic Pole Inversion Based on Molecular Field Theory

Shin-ichi Ohkoshi† and Kazuhito Hashimoto*,†,‡

Contribution from the Research Center for Advanced Science and Technology, The University of Tokyo, 4-6-1 Komaba, Meguro-ku, Tokyo153-8904, Japan, and Kanagawa Academy of Science and Technology, 3-2-1 Sakato, Takatsu-ku, Kawasaki, Kanagawa 213, Japan

Received May 4, 1999. Revised Manuscript Received September 17, 1999

Abstract: We show a novel magnetic phenomenon, "photoinduced magnetic pole inversion", which occurs even in the absence of an external magnetic field. The key of this strategy is to control the compensation temperature by a pure photoprocess. Here, we combined two magnetic behaviors which were developed recently. One of them is the photoinduced change of magnetization for some of the Prussian blue analogues. The other is a so-called mixed ferro-ferrimagnetism in the system of ternary metal Prussian blue analogues. We show a strategy to obtain this phenomenon based on molecular field (MF) theory and we design new classes of ternary metal Prussian blue analogues, $(Fe^{II}_xMn^{II}_{1-x})_{1.5}[Cr^{III}(CN)_6]\cdot zH_2O$, including photosensitive $Fe^{II}-Cr^{III}$ sites. Their magnetic properties, such as saturation magnetization, coercive field, Curie temperature, and compensation temperature, were controlled by changing the compositional factor x. When the material for $x = 0.40$ was irradiated by visible light under a weak external magnetic field (10 G), the photoinduced magnetization reversal occurred. This phenomenon can be simulated well by the MF theory considering only two types of superexchange couplings between the nearest neighbor sites, one for $Fe^{II}-Cr^{III}$ and the other for $Mn^{II}-Cr^{III}$.

I. Introduction

One of the targets in the field of magnetic materials is to develop new types of functionalized magnets. For example, magnetic materials exhibiting giant magnetic resistance effects open a new avenue in the field of magnetic memory devices.[1,2] Our objective in the present work is to control magnetic properties by photostimuli. The first observation of photoinduced magnetic effects was reported with Si-doped yttrium iron garnet (YIG) 30 years ago.[3−7] In this system, the initial permeability and coercive field were changed by photoirradiation. Conversely, we have recently reported a photoinduced enhancement of magnetization in $K_{0.4}Co^{II}_{0.3}Co^{III}[Fe^{II}(CN)_6]\cdot 5H_2O$.[8,9] In this material, the electron-transfer proceeds from Fe^{II} ($S = 0$) to Co^{III} ($S = 0$) by visible light irradiation, producing Fe^{III} ($S = 1/2$)−CN−Co^{II} ($S = 3/2$). We have also showed the visible light-induced magnetization decrease with $Fe^{II}_{1.5}[Cr^{III}(CN)_6]\cdot 7.5H_2O$.[10] In this material, the spin states of Fe^{II} ($t_{2g}{}^4e_g{}^2$) and Cr^{III} ($t_{2g}{}^3$) are not changed but the ferromagnetic coupling between these metal ions is disconnected by irradiation.

In the present work, we focus our attention on the optical-control of magnetic poles (N and S). In an optical magnetic memory media made of magnetic metals such as TbFe, the phenomenon of photothermally induced magnetic pole inversion is used. In this type of device, the magnetic material is heated above its Curie temperature (T_c) by a photothermal process in the presence of a reverse external magnetic field, and then, during the cooling process below T_c, the magnetization occurs parallel to the external magnetic field, resulting in a magnetic pole inversion.[11] In the present paper, we show a novel magnetic phenomenon "photoinduced magnetic pole inversion". This phenomenon occurs even in the absence of an external magnetic field. Therefore, its mechanism is completely different from that of the photothermally induced magnetic pole inversion.

The present novel phenomenon can be achieved by a combination of the photoinduced change of magnetization[10] and the mixed ferro-ferrimagnetism[12−16] developed recently. In the latter magnetism, the weight average of the ferromagnetic and ferrimagnetic characters can be precisely controlled by fine-tuning of the composition. One of the most important characteristics for this magnet is that the spin frustration does not occur, even though both signs of exchange interaction are incorporated. As a prototype of this magnetism, we succeeded in manipulating

* To whom correspondence should be addressed.
† The University of Tokyo.
‡ Kanagawa Academy of Science and Technology.

(1) Baibich, M. N.; Broto, J. M.; Fert, A.; Nguyen Van Dau, N.; Petroff, F.; Eitenne, P.; Creuxet, G.; Friedrich, A.; Chazelas, J. *Phys. Rev. Lett.* **1988**, *61*, 2472.
(2) Cieny, B.; Speriosu, V. S.; Psrkin, S. S. P.; Gurney, B. A.; Wilhoit, D. R.; Mauri, D. *Phys. Rev. B* **1991**, *43*, 1297.
(3) Teale, R. W.; Temple, D. W. *Phys. Rev. Lett.* **1967**, *19*, 904.
(4) Enz, U.; Van der Heide, H. *Solid State Commun.* **1968**, *6*, 347.
(5) Lems, W.; Rijnierse, P. J.; Bongers, P. F.; Enz, U. *Phys. Rev. Lett.* **1968**, *21*, 1643.
(6) Pearson, R. F.; Annis, A. D.; Kompfner, P. *Phys. Rev. Lett.* **1968**, *21*, 1805.
(7) Hisatake, K. *J. Appl. Phys.* **1977**, *48*, 2971.
(8) Sato, O.; Iyoda, T.; Fujishima, A.; Hashimoto, K. *Science* **1996**, *272*, 704.
(9) Sato, O.; Einaga, Y.; Iyoda, T.; Fujishima, A.; Hashimoto, K. *J. Electrochem. Soc.* **1997**, *144*, 11.
(10) Ohkoshi, S.; Einaga, Y.; Fujishima, A.; Hashimoto, K. *J. Electroanal. Chem.* **1999**, *473*, 245.
(11) Mallinson, J. C. *The Foundation of Magnetic Recording*; Academic Press: New York, 1993.
(12) Ohkoshi, S.; Iyoda, T.; Fujishima, A.; Hashimoto, K. *Phys. Rev. B* **1997**, *56*, 11642.
(13) Ohkoshi, S.; Hashimoto, K. *Phys. Rev. B.* In press.
(14) Ohkoshi, S.; Sato, O.; Iyoda, T.; Fujishima, A.; Hashimoto, K. *Inorg. Chem.* **1997**, *36*, 268.
(15) Ohkoshi, S.; Fujishima, A.; Hashimoto, K. *J. Am. Chem. Soc.* **1998**, *120*, 5349.
(16) Ohkoshi, S.; Abe, Y.; Fujishima, A.; Hashimoto, K. *Phys. Rev. Lett.* **1999**, *82*, 1285.

10.1021/ja991473c CCC: $18.00
Published on Web 11/03/1999

both ferromagnetic ($J_{NiCr} > 0$) and antiferromagnetic ($J_{MnCr} < 0$) superexchange interactions independently with the compounds in the series of $(Ni^{II}_xMn^{II}_{1-x})_{1.5}[Cr^{III}(CN)_6]\cdot 7.5H_2O$ ($0 \le x \le 1$).[12−14] Their magnetic properties such as the saturation magnetization (M_s), the coercive field (H_c), and the thermodynamics of magnetization including the compensation temperature (T_{comp}) could be controlled by fine-tuning the compositional factor x, without spin glass behavior. In addition, in $(Ni^{II}_aMn^{II}_b Fe^{II}_c)_{1.5}[Cr^{III}(CN)_6]\cdot zH_2O$ containing one antiferromagnetic interaction and two ferromagnetic interactions, we have recently succeeded in designing and synthesizing a novel magnet exhibiting two compensation temperatures, i.e., the spontaneous magnetization changes its sign twice with changing temperature.[16]

By a combination of this mixed ferro-ferrimagnetism and the photoinduced change of magnetization, we previously showed the first observation of photoinduced magnetic pole inversion using the $(Fe^{II}_{0.40}Mn^{II}_{0.60})_{1.5}[Cr^{III}(CN)_6]\cdot 7.5H_2O$ system.[17] To understand this novel phenomenon, we show here (1) the details of the strategy and model calculations based on the MF theory, (2) the structures and magnetic properties of the members for the $(Fe^{II}_xMn^{II}_{1-x})_{1.5}[Cr^{III}(CN)_6]\cdot zH_2O$ system, (3) the optomagnetic behaviors of this system, and (4) the theoretical analysis of their observed photomagnetic phenomenon based on the MF theory.

II. Strategy

First, we show the strategy of the photoinduced magnetic pole inversion. The key of our strategy is to control the compensation temperature (T_{comp})[18−25] in a pure photon process. To meet this challenge, the theoretical prediction of the thermodynamics is indispensable. However, for classical metal or metal oxide magnets, such a prediction is difficult in general. One of the reasons is that various types of exchange and/or superexchange interactions exist among metals or metal ions. Moreover, the metal substitution often causes structural distortions. Conversely, for Prussian blue analogues,[26−34] which are one of the most attractive classes of molecule-based magnets,[35−38] the theoretical treatment becomes much simpler for the following reasons: (1) The face-centered cubic (fcc) structure of the Prussian blue analogues is maintained even when metal ion substitution is carried out. (2) Only the superexchange interactions between the nearest neighbor metal ions can operate among spin sources. In other words, contributions from the second nearest neighbor sites can be neglected due to the relatively long distances (10 Å) between those metal ions.[12] Therefore, the design of novel magnets based on the simple MF theory is effective for Prussian blue analogues.

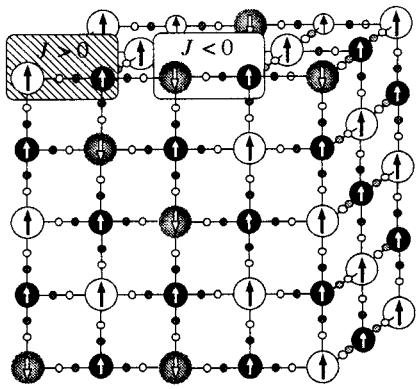

Figure 1. Schematic diagram illustrating mixed ferro-ferrimagnetism with both ferromagnetic ($J_{AB} > 0$) and antiferromagnetic ($J_{AB} < 0$) interactions. The carbon (small gray) ends of the cyano groups are bonded to B^{III} (black spheres), and the nitrogen (small white) ends are bonded to either $A1^{II}$ (white spheres) or $A2^{II}$ (gray spheres).

For ternary metal Prussian blue analogues, $(A1^{II}_xA2^{II}_{1-x})_{1.5}[B^{III}(CN)_6]$, the thermodynamics of spontaneous magnetization can be evaluated, considering only two types of superexchange couplings between the nearest neighbor sites, one for A1-B and the other for A2-B (Figure 1). The molecular fields H_{A1}, H_{A2}, and H_B acting on the three sublattice sites can be expressed as follows:

$$H_{A1} = H_0 + n_{A1B}M_B \quad (1)$$

$$H_{A2} = H_0 + n_{A2B}M_B \quad (2)$$

$$H_B = H_0 + n_{BA1}M_{A1} + n_{BA2}M_{A2} \quad (3)$$

where H_0 is the external magnetic field, n_{ij} are the molecular field coefficients, and M_{A1}, M_{A2}, and M_B are the sublattice magnetizations per unit volume for the A1, A2, and B sites, respectively. The molecular field coefficients n_{ij} are related to the exchange coefficients (J_{ij}) by

$$n_{ij} = \frac{2Z_{ij}}{\lambda_j N(g\mu_B)^2}J_{ij} \quad (4)$$

where μ_B is the Bohr magneton, Z_{ij} are the numbers of the nearest neighbor j-site ions surrounding an i-site ion [$Z_{A1B} = Z_{A2B} = 4$; $Z_{BA1} = 6x$; $Z_{BA2} = 6(1 - x)$], g is the g factor, N is the total number of all types of metal ions per unit volume, and λ_j presents the mole fractions for each metal ion per unit volume, i.e., $\lambda_{A1} = 1.5x$, $\lambda_{A2} = 1.5(1 - x)$, and $\lambda_B = 1$. The J_{ij} values can be obtained from the observed T_c values for elemental binary metal Prussian blue analogues: $A1^{II}_{1.5}[B^{III}(CN)_6]$ and $A2^{II}_{1.5}[B^{III}(CN)_6]$. If we designate the thermally averaged values of the spins of the metal ions in their respective sites in the direction of each sublattice magnetization as $\langle S_i \rangle$, the sublattice magnetization (M_i) can be expressed as follows:

(17) Ohkoshi, S.; Yorozu, S.; Sato, O.; I yoda, T.; Fujishima, A.; Hashimoto, K. *Appl. Phys. Lett.* **1997**, *70*, 1040.
(18) Néel, L. *Ann. Phys.* **1948**, *3*, 137.
(19) Gorter, E. W. *Philips Res. Rept.* **1954**, *9*, 295.
(20) Lotgering, F. K. *Philips Res. Rept.* **1956**, *11*, 190.
(21) Pauthenet, R. *J. Appl. Phys.* **1958**, *29*, 253.
(22) Lüthi, B. *Phys. Rev.* **1966**, *148*, 519.
(23) *Lndolt-Bernstein Neue Serie III/4b*; Springer-Verlag: Berlin, 1970.
(24) Mathoniére, C.; Nuttal, C. J.; Carling, S. G.; Day, P. *Inorg. Chem.* **1996**, *35*, 1201.
(25) Ren, Y.; Palstra, T. T. M.; Khomskii, D. I.; Pellegrin, E.; Nugroho, A. A.; Menovsky, A. A.; Sawatzky, G. A. *Nature* **1998**, *396*, 441.
(26) Hoden, A. N.; Matthias, B. T.; Anderson, P. W.; Luis, H. W. *Phys. Rev.* **1956**, *102*, 1463.
(27) Griebler, W. D.; Babel, D. Z. *Naturforsch., Teil B* **1982**, *87*, 832.
(28) Mallah, T.; Thiebaut, S.; Verdaguer, M.; Veillet, P. *Science* **1993**, *262*, 1554.
(29) Entley, W. R.; Girolami, G. S. *Inorg. Chem.* **1994**, *33*, 5165.
(30) Ferlay, S.; Mallah, T.; Ouahés, R.; Veillet, P.; Verdaguer, M. *Nature* **1995**, *378*, 701.
(31) William, R. E.; Girolami, G. S. *Science* **1995**, *268*, 397.
(32) Sato, O.; I yoda, T.; Fujishima, A.; Hashimoto, K. *Science* **1996**, *271*, 49.
(33) Verdaguer, M.; Mallah, T.; Gadet, V.; Castro, I.; Hélary, C.; Thiébaut, S.; Veillet, P. *Conf. Coord. Chem.* **1993**, *14*, 19.
(34) Ohkoshi, S.; Hashimoto, K. *Chem. Phys. Lett.* In press.
(35) Miller, J. S.; Epstein, A. J. *Angew. Chem., Int. Ed. Engl.* **1994**, *33*, 385.
(36) Kahn, O. *Molecular Magnetism;* VCH: New York, 1993.
(37) Gatteschi, D.; Kahn, O.; Miller, J. S.; Palacio, F., Eds. *Magnetic Molecular Materials*; Kluwer: Dordrecht, The Netherlands 1991.
(38) Palacio, F.; Antorrena, G.; Castro, M.; Burriel, R.; Rawson, J.; Smith, J. N. B. *Phys. Rev. Lett.* **1997**, *79*, 2336.

$$M_i = \lambda_i N g \mu_B \langle S_i \rangle \quad (5)$$

Substituting eqs 4 and 5 into eqs 1−3, we have

$$H_{A1} = H_0 + \frac{2Z_{A1B}J_{A1B}}{g\mu_B}\langle S_B \rangle \quad (6)$$

$$H_{A2} = H_0 + \frac{2Z_{A2B}J_{A2B}}{g\mu_B}\langle S_B \rangle \quad (7)$$

$$H_B = H_0 + \frac{2Z_{BA1}xJ_{A1B}}{g\mu_B}\langle S_{A1} \rangle + \frac{2Z_{BA2}(1-x)J_{A2B}}{g\mu_B}\langle S_{A2} \rangle \quad (8)$$

The magnitudes of $\langle S_i \rangle$, setting $H_0 = 0$, are given by

$$\langle S_i \rangle = S_{i_0} B_{S_i}\left(\frac{g\mu_B H_i S_{i_0}}{k_B T}\right) \quad (9)$$

where B_S is the Brillouin function, S_{i_0} is the value of $\langle S_i \rangle$ at $T = 0$ K and k_B is the Boltzmann constant. The $\langle S_i \rangle$ can be calculated numerically and then the sublattice magnetizations (M_i) in eq 5 are obtained. The total magnetization (M_{total}) can then be obtained by

$$(M_{total}) = M_{A1} - M_{A2} + M_B \quad (10)$$

Using this MF model, we can design the ternary metal Prussian blue analogues which exhibit negative magnetization, and predict their T_{comp} values.

For some Prussian blue analogues, we have shown that the spontaneous magnetization could be changed by photoirradiation. Therefore, by introducing such a photosensitive ferro (or ferri) magnet to the mixed ferro-ferrimagnet, the thermodynamics of the magnetization would be controlled by photoirradiation. That is, if the photoinduced magnetization change proceeds at either the ferromagnetic or ferrimagnetic site in mixed ferro-ferrimagnets, the balance of magnetization between the ferromagnetic and ferrimagnetic site will change, resulting in the photoinduced magnetic pole inversion. Let us show a model calculation of this concept using spin crossover phenomenon. Here, we consider the $(A1^{II}_xA2^{II}_{1-x})_{1.5}[B^{III}(CN)_6]$ magnet including a photosensitive site, in which the spin quantum numbers for the metal ions are $S_{A1} = 1$, $S_{A2} = 2$, and $S_B = 3/2$, and the J_{A1B} and J_{A2B} values are +5.0 and −2.5 cm^{-1}. The temperature dependence of magnetization for $x = 0.44$ can be calculated using eqs 1−10 as shown in the upper curve (i) of Figure 2a. This curve is composed of the positive magnetizations derived from the A1 and B sublattices and the negative magnetization from the A2 sublattice. When the spin crossover occurs at the A1 metal ion of a ferromagnetic site by photoirradiation ($S_{A1} = 1 \rightarrow S_{A1}' = 0$), the positive magnetization decreases and hence the magnetization reversal can occur as shown in the lower curve (ii) of Figure 2a. Similarly, the pole inversion can be expected, when the spin crossover occurs at the A2 metal ion of a ferrimagnetic site by photoirradiation ($S_{A2} = 2 \rightarrow S_{A2}' = 0$). In this case, we consider the member for $x = 0.36$, which shows a compensation temperature before irradiation (Figure 2b, lower curve (i)). When the spin crossover proceeds from $S_{A2} = 2$ to $S_{A2}' = 0$ at 20% of the A2 site, the magnetization curve changes to the upper curve (ii) in Figure 2b, showing the pole inversion at the temperature below T_{comp}. We can thus design the magnet exhibiting the photoinduced magnetic pole inversion. Of course, this novel phenomenon will occur not only by photoinduced spin crossover but also by various types of photoinduced phenomenon such as photoinduced charge transfer among metal ions and photoinduced change of superexchange interaction.

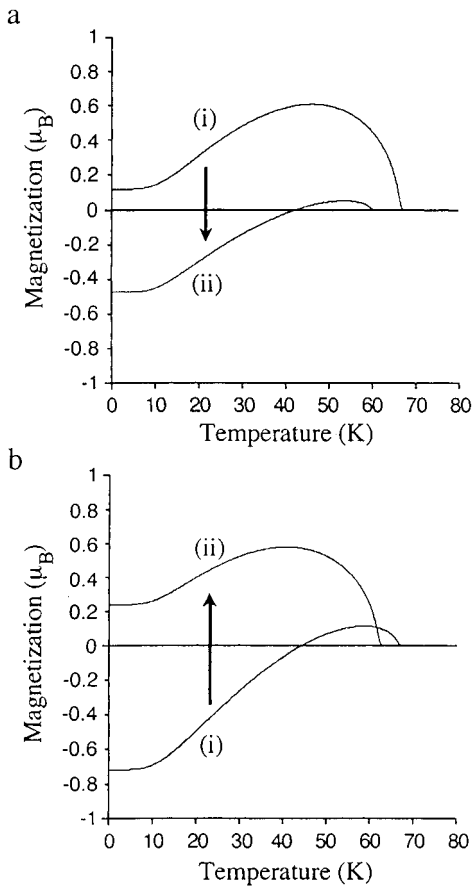

Figure 2. Model calculation of the photoinduced magnetic pole inversion. (a) Calculated temperature dependences of magnetization for $(A1^{II}_{0.44}A2^{II}_{0.56})_{1.5}[B^{III}(CN)_6]\cdot zH_2O$ ($S_{A1} = 1$, $S_{A2} = 5/2$, $S_B = 3/2$) based on the MF theory, with J coefficients $J_{A1B} = 5.0$ cm^{-1} and $J_{A2B} = -2.5$ cm^{-1}: (i) before and (ii) after the irradiation where 45% of A1 has been converted to the low-spin state. (b) Calculated temperature dependences of magnetization for $(A1^{II}_{0.36}A2^{II}_{0.64})_{1.5}[B^{III}(CN)_6]\cdot zH_2O$: (i) before and (ii) after the irradiation where 20% of A2 has been converted to the low-spin state.

As a prototype exemplifying our concept, we have designed a $(Fe_xMn_{1-x})_{1.5}[Cr(CN)_6]\cdot 7.5H_2O$ magnet containing both ferromagnetic (Fe−Cr) and antiferromagnetic (Mn−Cr) interactions. In this system, the magnetization of $Fe_{1.5}[Cr(CN)_6]\cdot 7.5H_2O$ for a ferromagnetic site is reduced by the visible light irradiation. Based on the Mössbauer experiments, we reported that this magnetization decrease is due to the photoinduced change of the J_{FeCr} value.[10] Conversely, the $Mn_{1.5}[Cr(CN)_6]\cdot 7.5H_2O$ for a ferrimagnetic site has no absorption in the visible region and hence does not change the magnetization by visible light irradiation. Using this mixed ferro-ferrimagnet, we demonstrate the photoinduced magnetic pole inversion.

III. Experimental Section

A. Synthesis. For the preparation of the Prussian blue analogues incorporating three different metal ions, $(Fe^{II}_xMn^{II}_{1-x})_{1.5}[Cr^{III}(CN)_6]\cdot zH_2O$, a 50 cm^3 aqueous solution (0.02 mol dm^{-3}) containing $FeCl_2$ and $MnCl_2$ was added to a concentrated aqueous solution (7 cm^3) of $K_3[Cr(CN)_6]$ (0.1 mol dm^{-3}), yielding a light brown colored microcrystalline powder. The precipitate was dialyzed for 48 h and then filtered. The fraction (x_{mix}) of Fe^{II} vs (Fe^{II} + Mn^{II}) in the above diluted aqueous solution was varied from 0 to 1, keeping the total metal ion concentration at 0.02 mol dm^{-3}. Elemental analyses for C, H, and N were carried out

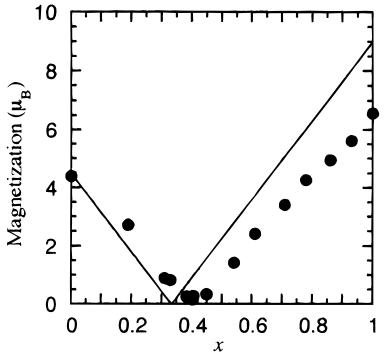

Figure 3. Calculated and experimentally observed saturation magnetizations for $(Fe^{II}_xMn^{II}_{1-x})_{1.5}[Cr^{III}(CN)_6]\cdot zH_2O$ as a function of x: calculated (—) and observed (●).

by standard microanalytical methods. Those for Mn, Fe, and Cr were analyzed by atomic absorption spectrometry.

B. Measurements. FT-IR spectra were recorded on a Biorad Model FTS 40A spectrometer. X-ray powder diffraction was measured on a Rigaku PW 1370 powder diffractometer. Magnetic susceptibility and magnetization measurements were carried out using a Quantum Design MPMS 7 superconducting quantum interference device (SQUID) magnetometer. A sample (~50 μg) supported on a commercial transparent adhesive tape was placed on the edge of an optical fiber. A weak blue light (360−450 nm, 2 mW/cm^2) of a Xe lamp was guided via an optical fiber into the SQUID magnetometer as an exciting light source.

IV. Results and Discussion

A. Structures. The elemental analyses for the synthesized complexes showed that the experimentally obtained x values were slightly larger than the x_{mix} values used in the syntheses, e.g., $x = 0.18$ ($x_{mix} = 0.10$), 0.60 ($x_{mix} = 0.50$), and 0.92 ($x_{mix} = 0.90$).[39] The CN stretching frequencies in the IR spectra for the resulting ternary metal complexes could not be assigned either to manganese cyanides (Mn^{II}−CN) or to iron cyanides (Fe^{II}−CN), but rather to chromium cyanides (Cr^{III}−CN). The X-ray powder diffraction patterns for all of the ternary complexes were consistent with the fcc structure. The lattice constant decreased successively from 10.78 to 10.64 Å with increasing x. In addition, their line widths were almost constant with the whole x. Therefore, we can conclude that the obtained materials are not physical mixtures of $Fe^{II}_{1.5}[Cr^{III}(CN)_6]\cdot 7.5H_2O$ and $Mn^{II}_{1.5}[Cr^{III}(CN)_6]\cdot 7.5H_2O$ powders, but are actual ternary metal complexes, $(Fe^{II}_xMn^{II}_{1-x})_{1.5}[Cr^{III}(CN)_6]\cdot 7.5H_2O$, in which Mn^{II} and Fe^{II} are randomly incorporated at nitrogen sites in the lattice.

B. Magnetic Properties. (a) Saturation Magnetization. The saturation magnetizations for $Fe^{II}_{1.5}[Cr^{III}(CN)_6]\cdot 7.5H_2O$ ($x = 1$) and $Mn^{II}_{1.5}[Cr^{III}(CN)_6]\cdot 7.5H_2O$ ($x = 0$) were 6.6 and 4.4 μ_B, respectively. The M_s values for the $(Fe^{II}_xMn^{II}_{1-x})_{1.5}[Cr^{III}(CN)_6]\cdot 7.5H_2O$ series showed a systematic change as a function of x. As seen in Figure 3, the observed M_s values for $0 < x < 0.4$ decreased linearly with increasing x. In contrast, above $x = 0.4$, the M_s values increased linearly with increasing x. The minimum M_s value, at x close to 0.4, was nearly zero. For the ternary metal Prussian blue analogues, parallel spins and antiparallel spins can partially or even completely cancel, depending on x. Therefore, using the spin quantum numbers for the metals ($S_{Fe} = 2$, $S_{Mn} = 5/2$, $S_{Cr} = 3/2$), together with x, the theoretical M_s values for the members of the series $(Fe^{II}_xMn^{II}_{1-x})_{1.5}[Cr^{III}(CN)_6]$ can be calculated by eq 11,[12] assuming the g factor of 2.

$$M_s = 2|S_{Cr} + 1.5[S_{Fe}x - S_{Mn}(1 - x)]| \qquad (11)$$

The calculated x dependence of the M_s value was similar to the observed one, indicating that these magnets were obtained without spin glass behavior and their magnetic properties are explained by the MF model described in section II. However, the experimental composition for the minimum M_s value was slightly different from the calculated one. One of the reasons is that the observed M_s value of 6.6 μ_B for $Fe^{II}_{1.5}[Cr^{III}(CN)_6]$ is smaller than the theoretical M_s value of 9.0 μ_B.

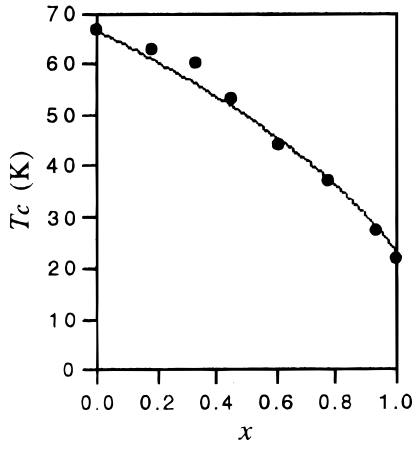

Figure 4. Plots of T_c values versus x for $(Fe^{II}_xMn^{II}_{1-x})_{1.5}[Cr^{III}(CN)_6]\cdot zH_2O$: calculated curve (—) based on eq 11 and observed (●).

(b) Curie Temperature. The T_c values of this series decreased monotonically from 67 to 21 K with increasing x, as shown in Figure 4. For binary metal Prussian blue analogues, $A_y[B(CN)_6]$, their theoretical T_c values are given by

$$T_c = \sqrt{C_A C_B n_{BA}{}^2} \qquad (12)$$

where C_i (i = A, B) are Curie constants; $C_i = \lambda_i N g^2 \mu_B{}^2 S_i(S_i + 1)/3k$.[12] Conversely, the theoretical T_c value for the present ternary metal Prussian blue analogues is expressed as follows:

$$T_c = \sqrt{C_{Fe}C_{Cr}n_{FeCr}{}^2 + C_{Mn}C_{Cr}n_{MnCr}{}^2} =$$

$$\sqrt{1.5S_{Cr}(S_{Cr}+1)\{xS_{Fe}(S_{Fe}+1)n_{FeCr}{}^2 + (1-x)S_{Mn}(S_{Mn}+1)n_{MnCr}{}^2\}} \qquad (13)$$

This equation shows that T_c varies as a function of a weighted average of molecular fields (n_{FeCr} and n_{MnCr}), and thus suggests that T_c changes continuously from the T_c value of $Mn^{II}_{1.5}[Cr^{III}(CN)_6]$ to that of $Fe^{II}_{1.5}[Cr^{III}(CN)_6]$ with increasing x.

(c) Compensation Temperature. Figure 5 shows the magnetization vs temperature curves at 10 G with various x values. The present materials exhibited various types of thermodynamics

(39) Analyses: Calcd for $Mn_{1.5}[Cr(CN)_6]\cdot 7.5H_2O$: Mn, 19.36; Cr, 12.22; C, 16.93; N, 19.75; H_2O, 31.74. Found: Mn, 19.13; Cr, 12.53; C, 16.68; N, 19.42; H_2O, 30.57. Calcd for $(Fe_{0.18}Mn_{0.82})_{1.5}[Cr(CN)_6]\cdot 6H_2O$: Fe, 3.73; Mn, 16.99; Cr, 13.04. Found: Fe, 3.77; Mn, 17.19; Cr, 12.72. Calcd for $(Fe_{0.33}Mn_{0.67})_{1.5}[Cr(CN)_6]\cdot 9H_2O$: Fe, 6.18; Mn, 12.10; Cr, 11.48. Found: Fe, 6.15; Mn, 12.04; Cr, 12.12. Calcd for $(Fe_{0.40}Mn_{0.60})_{1.5}[Cr(CN)_6]\cdot 7.5H_2O$: Fe, 7.94; Mn, 11.5; Cr, 12.2; C, 16.9; N, 19.7. Found: Fe, 8.03; Mn, 11.5; Cr, 11.9; C, 17.1; N, 19.7. Calcd for $(Fe_{0.42}Mn_{0.58})_{1.5}[Cr(CN)_6]\cdot 6.5H_2O$: Fe, 8.70; Mn, 11.63; Cr, 12.74. Found: Fe, 8.78; Mn, 11.74; Cr, 12.97. Calcd for $(Fe_{0.54}Mn_{0.46})_{1.5}[Cr(CN)_6]\cdot 8.5H_2O$: Fe, 10.15; Mn, 8.56 Cr, 11.70. Found: Fe, 10.17; Mn, 8.58; Cr, 12.45. Calcd for $(Fe_{0.60}Mn_{0.40})_{1.5}[Cr(CN)_6]\cdot 6.5H_2O$: Fe, 12.32; Mn, 8.06; Cr, 12.73. Found: Fe, 12.28; Mn, 8.03; Cr, 12.85. Calcd for $(Fe_{0.69}Mn_{0.31})_{1.5}[Cr(CN)_6]\cdot 6.5H_2O$: Fe, 14.08; Mn, 6.32 Cr, 12.73. Found: Fe, 14.19; Mn, 6.37; Cr, 13.10. Calcd for $(Fe_{0.76}Mn_{0.24})_{1.5}[Cr(CN)_6]\cdot 7H_2O$: Fe, 15.28; Mn, 4.70; Cr, 12.45. Found: Fe, 15.35; Mn, 4.72; Cr, 13.06. Calcd for $(Fe_{0.85}Mn_{0.15})_{1.5}[Cr(CN)_6]\cdot 7.5H_2O$: Fe, 17.09; Mn, 2.92; Cr, 12.45. Found: Fe, 17.12; Mn, 2.92; Cr, 13.02. Calcd for $(Fe_{0.92}Mn_{0.08})_{1.5}[Cr(CN)_6]\cdot 8H_2O$: Fe, 17.70 Mn, 1.49; Cr, 11.93. Found: Fe, 17.87; Mn, 1.51; Cr, 12.54. Calcd for $Fe_{1.5}[Cr(CN)_6]\cdot 7.5H_2O$: Fe, 19.62; Cr, 12.18; C, 16.88; N, 19.69; H, 3.5. Found: Fe, 19.6; Cr, 12.4; C, 16.9; N, 20.2; H, 3.2.

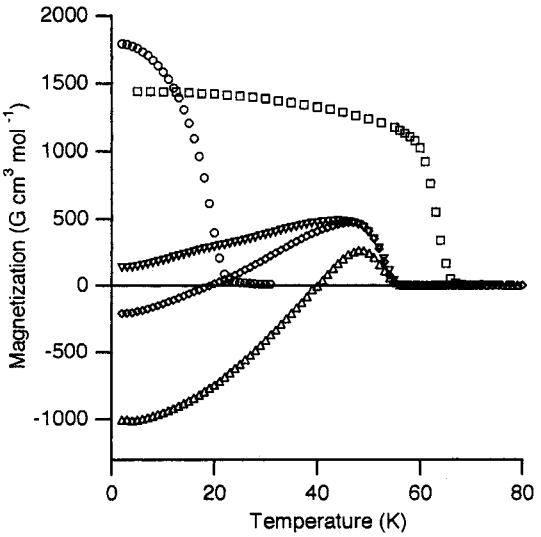

Figure 5. Magnetization versus temperature curves of $(Fe^{II}_xMn^{II}_{1-x})_{1.5}[Cr^{III}(CN)_6]\cdot zH_2O$ observed at 10 G: (□) $x = 0$; (▽) $x = 0.38$; (◇) $x = 0.40$; (△) $x = 0.42$; and (○) $x = 1$.

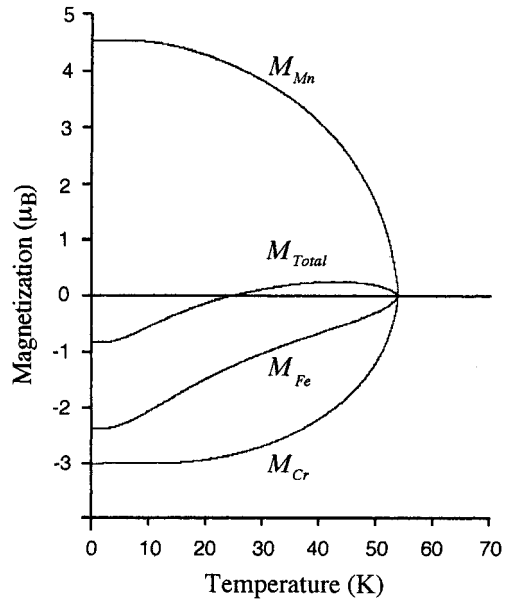

Figure 6. Calculated temperature dependence curves for each sublattice (M_M, M_{Fe}, M_{Cr}) and total magnetization (M_{total}) for $(Fe^{II}_{0.40}Mn^{II}_{0.60})_{1.5}[Cr^{III}(CN)_6]$ based on the three-sublattice molecular field theory.

of magnetization, depending on x. Particularly, the materials where x was 0.40−0.42 exhibited negative magnetization below T_{comp}. These various types of temperature dependence of the magnetization and compensation temperatures could be understood based on the MF model, by considering only the superexchange interactions between the nearest neighbors (Fe^{II}−Cr^{III} and Mn^{II}−Cr^{III}). These magnetic phenomena arise because the positive magnetization due to the Mn^{II} sublattice and the negative magnetizations due to the Fe^{II} and Cr^{III} sublattices have different temperature dependences. As an example, Figure 6 shows the calculated thermodynamics of sublattice and total magnetizations for $x = 0.40$. For this composition, the relations of the magnitude among the sublattice magnetizations are expressed as follows: $|M_{Fe} + M_{Cr}| < |M_{Mn}|$ at $T > T_{comp}$ and $|M_{Fe} + M_{Cr}| > |M_{Mn}|$ at $T < T_{comp}$.[40]

(d) Coercive Field. The coercive field (H_c) is a significant parameter for the present work because negative magnetization below T_{comp} must be maintained under external magnetic field.

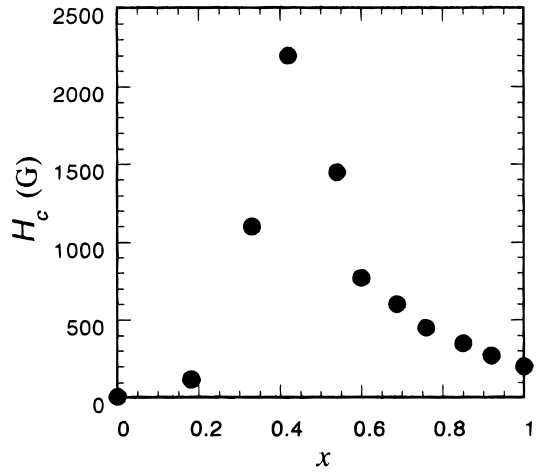

Figure 7. Coercive fields of $(Fe^{II}_xMn^{II}_{1-x})_{1.5}[Cr^{III}(CN)_6]\cdot zH_2O$ as a function of x observed at 5 K.

Fortunately, the H_c values for the magnets exhibiting compensation temperatures were much larger than an applied external magnetic field of 10 G (Figure 7). Especially, H_c values for the magnets where x was close to 0.4 were much larger than those at other x values, e.g., 6 ($x = 0$), 2200 ($x = 0.42$), and 200 G ($x = 1$). In general, the H_c value depends on the grain size of the sample. However, if the grain sizes are nearly the same, the H_c values are expected to be proportional to the M_s^{-1} values.[41] This relation was observed with the series of $(Ni^{II}_xMn^{II}_{1-x})_{1.5}[Cr^{III}(CN)_6]\cdot 7.5H_2O$.[12] The same holds true for the series of the present $(Fe^{II}_xCr^{II}_{1-x})_{1.5}[Cr^{III}(CN)_6]\cdot zH_2O$ system.

C. Photoinduced Magnetic Pole Inversion. We demonstrate the photoinduced magnetic pole inversion using the $(Fe^{II}_xMn^{II}_{1-x})_{1.5}[Cr^{III}(CN)_6]\cdot 7.5H_2O$ system. Let us first show the photomagnetic effect of the elemental compounds, $Fe^{II}_{1.5}[Cr^{III}(CN)_6]\cdot 7.5H_2O$ ($x = 1$) ferromagnet and $Mn^{II}_{1.5}[Cr^{III}(CN)_6]\cdot 7.5H_2O$ ($x = 0$) ferrimagnet. A visible light-induced magnetization decrease occurred with $Fe^{II}_{1.5}[Cr^{III}(CN)_6]\cdot 7.5H_2O$.[10] By irradiation with a filtered blue light (360−450 nm, 2 mW cm^{-2}) at 5 K, for example, ca. 10% of magnetization was decreased for 8 h of irradiation at 10 G (Figure 8). This reduced magnetization persisted for a period of several days at 5 K after turning off the light. The magnetic property of this irradiated sample returned to the initial one when the temperature of the sample was raised above 40 K, showing that the magnetization can be reduced by a photon mode and recovered by a thermal mode repeatedly. According to the Mössbauer experiments, the spin state of $Fe^{II}_{1.5}[Cr^{III}(CN)_6]\cdot 7.5H_2O$ is not changed by the photoirradiation.[10] Therefore, this photoinduced magnetization decrease will be due to the change of the superexchange interaction between Fe^{II} and Cr^{III}. The photoexcited state is the mixed valence state of Cr^{III}−CN−Fe^{II} and Cr^{II}−CN−Fe^{III}, which relax to a metastable state immediately where the ferromagnetic interaction is too weak to maintain the spin ordering. This metastable state returns to the original ferromagnetic state above 40 K. Conversely, the $Mn_{1.5}[Cr(CN)_6]\cdot 7.5H_2O$ for a ferrimagnetic site has no absorption in the visible region and hence did not show any change of magnetization by the visible light irradiation.

(40) The observed magnetization values were smaller than the calculated ones. This is because the calculated spontaneous magnetizations are essentially the saturated values, as the MF theory does not consider the magnetization process. In the experiment, however, the observed magnetization depends on the external magnetic field and the values obtained in the present experiment are not saturated ones.

(41) Chikazumi, S. *Physics of Magnetism*; J. Wiley & Sons: New York, London and Sydney, 1964; p 357.

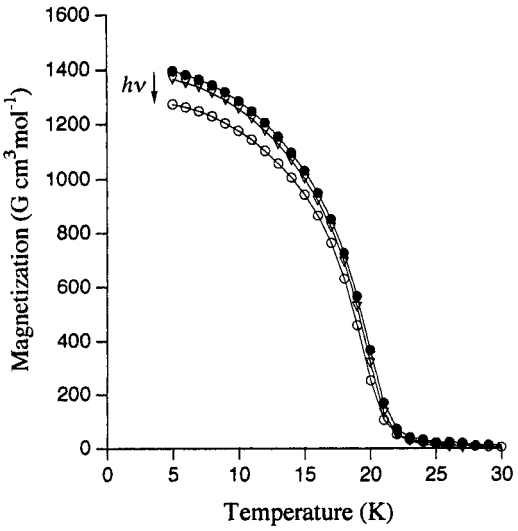

Figure 8. Magnetization versus temperature curves of $Fe^{II}_{1.5}[Cr^{III}(CN)_6]\cdot zH_2O$ observed at $H = 10$ G before (●) and after (○) light irradiation. The curves before irradiation and after irradiation are field cooling and field heating magnetization curves, respectively. Magnetic measurement sequence: 30 K → ● → 5 K (light irradiation) → ○ → 30 K → 80 K (thermal treatment) → 30 K → ▽ → 5 K.

To demonstrate the photoinduced magnetic pole inversion phenomenon, we chose $(Fe^{II}_{0.40}Mn^{II}_{0.60})_{1.5}[Cr^{III}(CN)_6]\cdot 7.5H_2O$, which exhibits a negative magnetization ($T_{comp} = 19$ K). When this sample was irradiated at 16 K with the filtered blue light (360−450 nm), the negative magnetization at 16 K gradually became positive under an existing external field of 10 G (Figure 9a). Simultaneously, the T_{comp} value shifted to a smaller value (19 K → 13 K → 7 K) and finally disappeared as shown in Figure 9b. This inverted magnetic pole persisted for a period of several days at 16 K after turning off the light. The magnetic pole inversion phenomenon is a photoinduced effect and not due to the heating of the sample under illumination. This is because, in the dark, the magnetization under 10 G did not vary at all by a slight change of the temperature; e.g. 16 K → 20 K → 16 K. The present novel phenomenon can be reasonably explained by the fact that the ratio of the ferromagnetic part (Fe−Cr site) to the ferrimagnetic part (Mn−Cr site) of magnetization changed due to the decrease of magnetization in the ferromagnetic sites. Moreover, the magnetization vs temperature curve was recovered by warming to 80 K. The magnetic pole inversion thus can be induced repeatedly by alternate optical and thermal stimulations.

To proceed, the photoinduced magnetic pole inversion under the present experimental condition needs a rather long time irradiation. One of the main reasons could be a very low quantum yield of the photoreaction. Another reason comes from the weak light intensity (2 mW/cm^2) used here to avoid raising the temperature of the sample during the measurement in the SQUID. By increasing the light intensity, the reaction rate can be increased. Especially when a pulsed laser is used as the light source, the rate may increase drastically because the present phenomenon will be based on a cooperative interaction among spin sources.

D. Simulation with MF Theory. The present photoinduced magnetic pole inversion can be simulated by using the MF model. First we analyze the photoinduced magnetization decrease of $Fe_{1.5}[Cr(CN)_6]\cdot 7.5H_2O$. From the results of ^{57}Fe Mössbauer measurements, we know that the spin state of Fe^{II} does not change by irradiation and that neither electron transfer nor spin transition occur photochemically, but the ferromagnetic

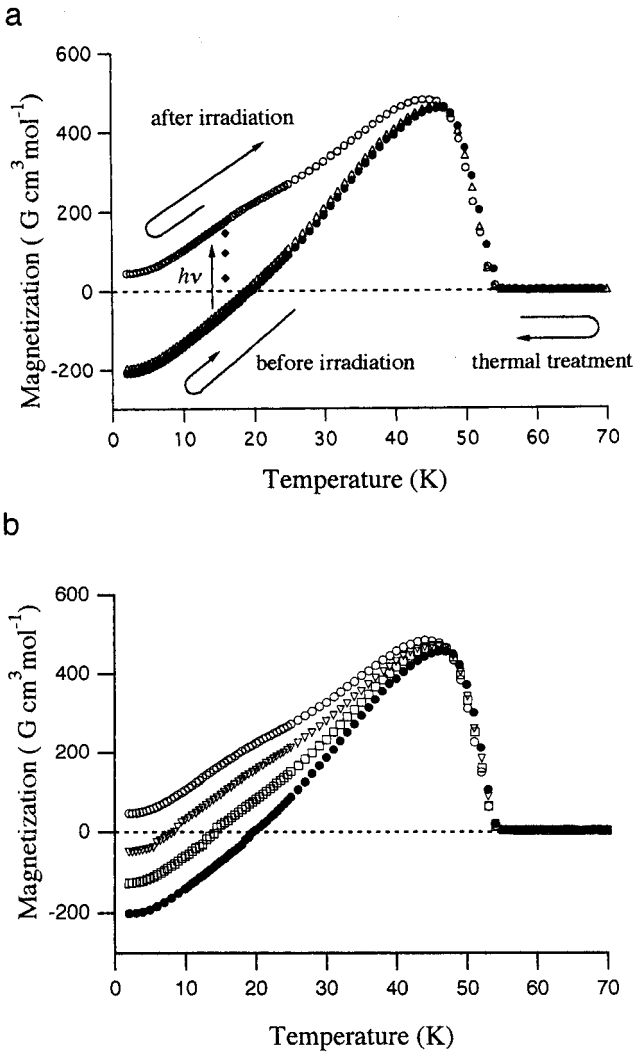

Figure 9. (a) Magnetization versus temperature curves of $(Fe^{II}_{0.40}Mn^{II}_{0.60})_{1.5}[Cr^{III}(CN)_6]$ observed at 10 G before (●) and after (○) light irradiation at 16 K for 72 h. The magnetic pole inversion is observed below the compensation temperature of 19 K by the light irradiation and the pole is reversed back again by warming it (△) to 80 K. Magnetic measurement sequence: 70 K → ● → 2 K → ● → 16 K (light irradiation for 6, 24, 48, 72 h; ◆) → ○ → 2 K → ○ → 70 K → 80 K (thermal treatment) → 70 K → △ → 2 K. (b) Magnetization versus temperature curves of $(Fe^{II}_{0.40}Mn^{II}_{0.60})_{1.5}[Cr^{III}(CN)_6]$ at 10 G in the field of $H = 10$ G before (●) and after light irradiation at 16 K for (□) 6, (▽) 24, and (○) 72 h.

coupling of Fe^{II} and Cr^{III} is disconnected by irradiation.[10] In other words, the ferromagnetic Fe^{II} metal ions were changed to paramagnetic ions by photoirradiation. Therefore, we assume that the ferromagnetic coupling between the Fe^{II} ion and the surrounding Cr^{III} ions is disconnected. Then the molecular fields H_{Fe}, H_{Fe}', and H_{Cr} acting on the sublattice sites after irradiation can be expressed as follows:

$$H_{Fe} = H_0 + n_{FeCr}M_{Cr} \quad (14)$$

$$H_{Fe}' = H_0 + n_{FeCr}'M_{Cr} \quad (15)$$

$$H_{Cr} = H_0 + n_{CrFe}M_{Fe} + n_{CrFe}'M_{Fe} \quad (16)$$

where the n_{ij} and n_{ij}' are the molecular field coefficients of nonconverted and photoconverted sites, respectively, relating to the exchange coefficients (J_{ij} and J_{ij}'). The J_{FeCr} value of 0.9 cm^{-1} before irradiation can be obtained from the experimental

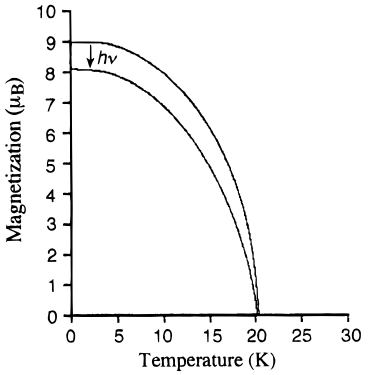

Figure 10. Simulation of the photoinduced magnetization decrease for $Fe^{II}_{1.5}[Cr^{III}(CN)_6]$ based on the MF theory. Upper and lower curves are the calculated temperature dependences of magnetization before and after the irradiation, respectively, based on eqs 14−16.

T_c value of 21 K, and the J_{FeCr}' value is assumed to be zero. We also have to take into consideration a spatial distribution of the photoconverted site, because the concentration of the disconnected sites may be lower at deeper sites from the surface according to the Lambert−Beer's law ($I/I_0 = 10^{-\alpha d}$, where α is an absorption coefficient of 3×10^3 and d is the distance from the surface). Using these conditions, the temperature dependences of the spontaneous magnetization before and after irradiation were evaluated theoretically as shown in Figure 10. These calculated curves qualitatively agree with the experimental ones.

We next simulate the photoinduced magnetization reversal of the material for $x = 0.40$, by a combination of the theoretical treatment for the photoinduced change of magnetization and that for ternary metal Prussian blue analogues. The molecular fields H_{Fe}, H_{Fe}', H_{Mn}, and H_{Cr} acting on each sublattice site in $(Fe_xMn_{1-x})_{1.5}[Cr(CN)_6]\cdot zH_2O$ can be expressed as follows:

$$H_{Mn} = H_0 + n_{MnCr}M_{Cr} \quad (17)$$

$$H_{Fe} = H_0 + n_{FeCr}M_{Cr} \quad (18)$$

$$H_{Fe}' = H_0 + n_{FeCr}'M_{Cr} \quad (19)$$

$$H_{Cr} = H_0 + n_{CrMn}M_{Mn} + n_{CrFe}M_{Fe} + n_{CrFe}'M_{Fe}' \quad (20)$$

The J_{MnCr} value of -2.5 cm^{-1} is obtained from the experimental critical temperature of $Mn^{II}_{1.5}[Cr^{III}(CN)_6]\cdot 7.5H_2O$ ($T_c = 67$ K). Under these conditions, the temperature dependence of the total magnetization of $(Fe^{II}_{0.40}Mn^{II}_{0.60})_{1.5}[Cr^{III}(CN)_6]\cdot 7.5H_2O$ before irradiation was calculated as shown in Figure 11. This calculated curve is consistent with the experimental curve qualitatively, although its T_{comp} value is slightly larger. Then, the magnetization vs temperature curve after irradiation was evaluated under similar conditions to the photoinduced magnetization decrease of $Fe^{II}_{1.5}[Cr^{III}(CN)_6]\cdot 7.5H_2O$. The calculated curve agreed with the experimentally obtained curve qualitatively. This correspondence shows that the present magnetic pole inversion is obtained according to our strategy. That is, the photoinduced magnetization change proceeds at the ferromagnetic site in the mixed ferro-ferrimagnet, and the balance of magnetization between the ferromagnetic and ferrimagnetic site changes, resulting in the photoinduced magnetic pole inversion.

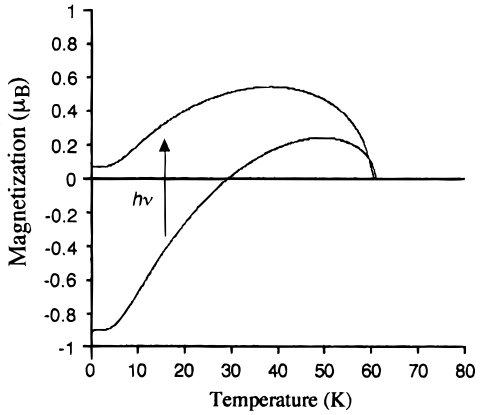

Figure 11. Simulation of the photoinduced magnetic pole inversion for $(Fe^{II}_{0.40}Mn^{II}_{0.60})_{1.5}[Cr^{III}(CN)_6]$ based on the MF theory. Lower and upper curves are the calculated temperature dependences of magnetization before and after the irradiation, respectively, based on eqs 17−20.

V. Conclusion

We have demonstrated the photoinduced magnetic pole inversion in a ferro-ferrimagnet $(Fe^{II}_xMn^{II}_{1-x})_{1.5}[Cr^{III}(CN)_6]\cdot 7.5H_2O$, by a combination of mixed ferro-ferrimagnetism and photomagnetism. Although the mechanism of the photoinduced process is not very clear, we can purpose the design of the novel magnets based on the MF theory. The present phenomenon occurs only at very low temperature (<19 K). This is due to the low T_c value of the molecule-based magnets used here. However, by designing the spin sources and the structure of compounds, the T_c value of Prussian blue analogues increases gradually.[42−44] For example, very recently, Girolami et al. and Miller et al. have succeeded in preparing $K^IV^{II}[Cr^{III}(CN)_6]$ with $T_c = 103$ °C and $K^I_{0.058}V^{II/III}[Cr^{III}(CN)_6]_{0.79}(SO_4)_{0.058}\cdot 0.93H_2O$ with $T_c = 99$ °C, respectively.[43,44] We have also succeeded in obtaining $K^I_{0.61}V^{II}[Cr^{III}(CN)_6]_{0.87}\cdot 7.0H_2O\cdot 0.4C_2H_5OH$ film ($T_c = 72$ °C) by using the electrochemical method.[45] We thus believe that a room-temperature photoinduced magnetic pole inversion is possible in the future, by applying the present strategy to those high T_c molecule-based magnets.

JA991473C

(42) Dujardin, E.; Ferlay, S.; Phan, X.; Desplanches, C.; Cartier dit Moulin, C.; Sainctavit, P.; Baudelet, F.; Dartyge, E.; Veillet. P.; Verdaguer, M. *J. Am. Chem. Soc.* **1998**, *120*, 11347.
(43) Holmes, S. M.; Girolami, G. S. *J. Am. Chem. Soc.* **1999**, *121*, 5593.
(44) Hatlevik, Ø.; Bushmann, W. E.; Zhang, J.; Manson, J. L.; Miller, J. S. *Adv. Mater.* **1999**, *11*, 914.
(45) Ohkoshi, S.; Mizuno, M.; Hung, G. J.; Fujishima, A.; Hashimoto, K. Unpublished results.